



HAL
open science

Study on Rotational and Unclogging Motions of Magnetic Chain-Like Microrobot

Karim Belharet, David Folio, Antoine Ferreira

► **To cite this version:**

Karim Belharet, David Folio, Antoine Ferreira. Study on Rotational and Unclogging Motions of Magnetic Chain-Like Microrobot. IEEE/RSJ International Conference on Intelligent Robots and Systems, Sep 2014, Chicago, IL, United States. pp.1-6. hal-01075291

HAL Id: hal-01075291

<https://hal.science/hal-01075291>

Submitted on 17 Oct 2014

HAL is a multi-disciplinary open access archive for the deposit and dissemination of scientific research documents, whether they are published or not. The documents may come from teaching and research institutions in France or abroad, or from public or private research centers.

L'archive ouverte pluridisciplinaire **HAL**, est destinée au dépôt et à la diffusion de documents scientifiques de niveau recherche, publiés ou non, émanant des établissements d'enseignement et de recherche français ou étrangers, des laboratoires publics ou privés.

Study on Rotational and Unclogging Motions of Magnetic Chain-Like Microrobot

Karim Belharet¹, David Folio² and Antoine Ferreira²

Abstract—Magnetic microrobotics was nowadays one of the most advanced technique to reach deep locations in human body for future biomedical applications. Different magnetic microrobot designs were proposed, such as bead pulling or microswimmers. In this paper, the use of chain-like of magnetic N -microspheres was investigated to enable new kind of motions and applications. An accurate theoretical model of chain-like magnetic microbeads navigating in viscous fluidic environments is described. Thus, the behavior of such microrobot was analyzed for different number of microspheres (ranging from $N = 2$ to 5). The efficiency of the proposed technique was demonstrated experimentally in a microfluidic vessel phantom to mimic atherosclerosis disease leading to plaque formation that fully occluded a vasculature.

I. INTRODUCTION

Design of integrated devices with electrical, mechanical, chemical or biological components at microscale enables numerous opportunities to improve on broad range of applications of technology, science and medicine [1]. In particular, it is well established that such microsystem can be used in many biomedical applications including minimally invasive surgical procedures [2]. Hence, when these microrobots are propelled in fluidic environments, especially in the blood circulatory system, a very large number of remote locations in the human body become accessible. Although there are different actuation methods proposed in the literature, the use of external magnetic fields has many advantages that circumvent the need for delivering power to the device and ensuring autonomous untethered motion of the microrobot [1], [3], [2]. Indeed, it has been shown that the coils of a clinical MRI system can be used to control untethered magnetic beads in 3D directions [4], [5], [6]. Nevertheless, it is still challenging to overcome some MRI-based navigation constraints (eg. pulsatile flow, variation of time-multiplexed sequence parameters, duty cycle of the propulsion gradients, and repetition time of the tracking sequence, availability, etc.) [7]. To overcome these limitations, several magnetic propulsion mainly based on the induction of magnetic force and torque. As example, different magnetic microrobot designs are proposed in the literature based on biologically inspired motion, such as helical microswimmer [8], [9], or beating flagella microswimmer [10], [11]. Such configuration is suitable in arterioles and capillaries [12], or for small swimmers size [3], [13]. Another magnetic microrobot design based

on magnetic microsphere, and referred as bead pulling [14], [15], is more useful to navigate in vessels where the drag is important as in arteries [12].

In this paper, we aim to investigate the use of a magnetic chain-like microrobot composed of microspheres that navigate within a microfluidic chip. Actually, thanks to its shape anisotropy, such configuration enables the generation of a magnetic torque together with the magnetic gradient pulling. Therefore, different range of biomedical applications could be investigated, such as cargo-towing [16], vessel cleaning or embolization [2]. Thus, this work focus on conveying a chain of magnetic microspheres (termed chain-like microrobot) in a microfluidic environment for innovative in-place blood vessel cleaning. Indeed, the cardiovascular system could be blocked due to atherosclerosis or peripheral vascular disease. These arterial occlusive diseases (AOD) are characterized by plaques formation along the vessel wall, implying vessel narrowing up to occlusion, and may lead to a heart attack or stroke. AOD treatment can be categorized into chemical or mechanical methods. In case of low narrowing pharmaceutical drugs (such as anticoagulants, anti-cholesterol, β -blocker, etc.) is usually the most suitable medical therapy. Otherwise, or if an ischemic attack or a stroke already is happened, surgical intervention are recommended. Here, we consider the use of magnetic microrobot to scrape and unclog fully occluded arteries.

This paper is organized as follow. First, in Section II the modeling of a magnetic chain of microspheres in viscous flow is presented. Then, the experimental setup is briefly described in Section III. Hence, the rotational behaviors of the chain-like microrobot are first characterized in a free extends in Section IV. Then, in Section V, an unclogging strategy for fibrous plaque removal is presented. Experiments demonstrate the relevance of the proposed techniques, and the use of chain-like agglomerates as magnetic microrobot for future biomedical application. This paper is concluded in Section VI.

II. MODELING OF MAGNETIC MICROROBOT NAVIGATING IN VISCOUS FLOW

A. Magnetic Properties of Agglomerates of Microrobot

Magnetic materials that are embedded into the magnetic microrobot can be divided into different classes, commonly referred as diamagnets, paramagnets, superparamagnets and ferromagnets. Especially, ferromagnetic materials give rise to large spontaneous magnetizations, and it is usually 10^4 times larger than would appear otherwise. Furthermore, in ferromagnetic materials one often sees hysteresis, as illustrated

¹Karim Belharet is with Hautes Études d'Ingénieur campus Centre, PRISME EA 4229, Châteauroux, France karim.belharet@hei.fr

²David Folio and Antoine Ferreira are with INSA Centre Val de Loire, Université d'Orléans, PRISME EA 4229, Bourges, France {david.folio, antoine.ferreira}@insa-cvl.fr

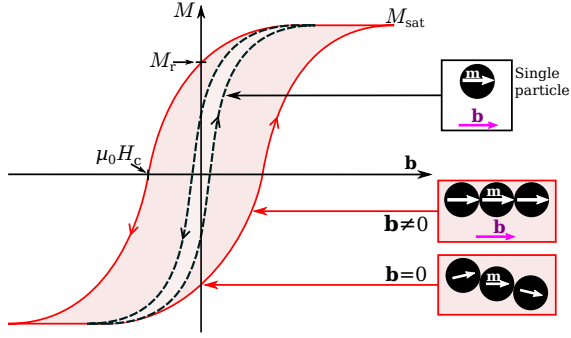


Fig. 1. Magnetic response of ferromagnetic material for single particle (dashed line), and particle aggregation (red line).

in Fig. 1. The shape of these hysteresis loops are related to the microrobot size [17]: in small particle (e.g. in the order of micron size) there is a single domain ground state which leads to a narrow hysteresis loop; while in larger or in chain of particles there is a multi-domain ground state which leads to a broad hysteresis loop. Moreover, the hysteresis magnetization characteristic of ferromagnetic microrobot exhibit, after the removal of the magnetic field, a non-zero remnant magnetization M_r . As a consequence, when exposed to an external magnetic field, the magnetic microparticles acquire a magnetic dipole moment and coalesce, under the influence of the magnetic dipole interaction, into a supraparticle structure (SPS), consisting of chain-like structures along the magnetic field direction, as depicted in the inset at $\mathbf{b} \neq 0$ in Fig. 1. Once the magnetic field vanish ($\mathbf{b} = 0$) remnant magnetization M_r allows to maintain the SPS cohesion.

B. Magnetic Manipulation

The basic principle of magnetic actuation is to manipulate a magnetic field \mathbf{b} to induce a magnetic force (\mathbf{f}_m) or torque (\mathbf{t}_m) on a magnetized microrobot. The magnetized material will then experience the following magnetic force (cf. Fig. 2-a):

$$\mathbf{f}_m = V(\mathbf{m} \cdot \nabla)\mathbf{b} \quad (1)$$

where V is the magnetic volume of the magnetic material, \mathbf{m} is the microrobot's magnetization (or equivalently the magnetic moment per volume), \mathbf{b} is the magnetic field and ∇ the gradient operator. The magnetic torque that acts to align the magnetization \mathbf{m} of the magnetic microrobot with the external magnetic field \mathbf{b} is defined as (see Fig. 2-b):

$$\mathbf{t}_m = V(\mathbf{m} \times \mathbf{b}) = V\|\mathbf{m}\| \|\mathbf{b}\| \sin \theta \quad (2)$$

with θ the lag between the magnetic microrobot magnetization direction and the magnetic field, as illustrated in Fig. 2. Let us notice that the magnetic force \mathbf{f}_m is related to the magnetic gradient $\nabla\mathbf{b}$, whereas the magnetic torque \mathbf{t}_m is dependent on the magnetic field \mathbf{b} . Therefore, in a uniform magnetic field, a microrobot will not experience any force until the magnetization \mathbf{m} is collinear with \mathbf{b} . Then, the magnetic torque \mathbf{t}_m vanish and the microrobot remains immobile. To actuate a magnetic microrobot, the magnetic field has to change spatially (e.g. thanks to a gradient field)

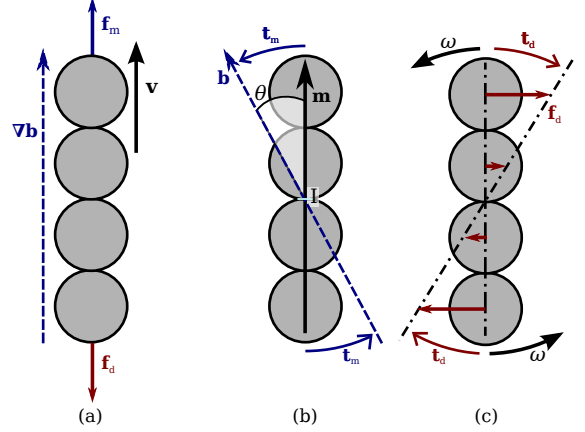


Fig. 2. Magnetic motion of a chain-like microrobot composed of 4-spheres: (a) steering motion using magnetic gradient $\nabla\mathbf{b}$; (b) rotational motion thanks to magnetic torque \mathbf{t}_m , and (c) the influence of the drag force \mathbf{f}_d and torque \mathbf{t}_d on the microrobot with an angular velocity ω .

or temporally, such as using rotating or oscillating field. Such various magnetic manipulation allows the design of a number of microrobotic systems with different actuation principles [8]–[11] for biomedical applications [2], [13].

C. Microrobot Motion in Viscous Flow

When a microrobot navigate in a viscous flow, it will experience a drag force (\mathbf{f}_d) and torque (\mathbf{t}_d), which are defined in the general 3D case by:

$$\begin{pmatrix} \mathbf{f}_d \\ \mathbf{t}_d \end{pmatrix} = - \begin{pmatrix} \mathbf{A} & \mathbf{B} \\ \mathbf{C} & \mathbf{D} \end{pmatrix} \begin{pmatrix} \mathbf{v} \\ \omega \end{pmatrix}, \quad (3)$$

with \mathbf{v} the linear velocity, and ω the angular velocity of the microrobot. The parameters \mathbf{A} , \mathbf{B} , \mathbf{C} and \mathbf{D} are 3×3 matrix function of the microrobot shape and the flow viscosity. Furthermore, these parameters have some symmetric properties related to the microrobot geometry. For instance, if the body shape has three orthogonal symmetric planes (such as spheroid, cuboid, or chain-like arrangement) we get $\mathbf{B} = \mathbf{C} = 0$. Particularly, in the case of spherical microrobot of radius r in a Stokes flow leads to:

$$\mathbf{A} = 6\pi\eta r \cdot \mathbb{I}_3, \text{ and } \mathbf{D} = 8\pi\eta r^3 \cdot \mathbb{I}_3 \quad (4)$$

where \mathbb{I}_3 defines the identity matrix, and η the flow viscosity.

The hydrodynamic behavior of spherical particles (4) has been deeply validated by many numerical and experimental studies for the drag force [18] and torque [19]. The drag force experienced by a non-spherical object has been also considered for spheroids, cylinders, chain of spheres, cuboid [20], [21], clusters of spheres [22], [23]. Classically, the drag force experienced by a non-spherical microrobot acts in the direction of the velocity \mathbf{v} , and is defined as follow:

$$\mathbf{f}_d = -6\pi\eta r_e \kappa_f \cdot \mathbf{v} \quad (5)$$

where κ_f is the dimensionless dynamic shape factor, and r_e is the *equivalent radius* defined as the radius of a sphere equal in volume to the non-spherical microrobot.

In contrast, fewer studies on the drag torque of non-spherical object have been carried out, and mainly numerical investigations are available using boundary element method (BEM) [24], multipole expansion method (MEM) [23], or Lattice Boltzmann method (LBM) [25], mirroring immersed boundary (MIB) [26]. In the same way as drag force (5), the drag torque on a rotating non-spherical microrobot is characterized by:

$$\mathbf{t}_d = -8\pi\eta r_e^3 \boldsymbol{\kappa}_{\text{rot}} \cdot \boldsymbol{\omega} \quad (6)$$

where $\boldsymbol{\kappa}_{\text{rot}}$ is the dimensionless rotational shape factor.

D. Drag Force and Torque on Chain-Like Microrobot

In this work, we aim to investigate the use of an agglomerate of magnetic microsphere (termed chain-like microrobot) that navigate in viscous flow. Chain of spheres arrangements have been theoretically well-investigated, allowing application of the boundary element method (BEM) [24], multipole expansion method (MEM) [23], Lattice Boltzmann method (LBM) [25], mirroring immersed boundary (MIB) [26]. Especially, Geller *et al.* have correlated their BEM results to compute the dynamic shape factor of a chain of N -spheres, and have proposed the following formula [24]:

$$\kappa_{f\perp} = \frac{4}{3}N^{2/3} \left(\log(2N) + 0.26269 + \frac{0.38185}{\log^2(2N)} \right)^{-1} \quad (7)$$

$$\kappa_{f\parallel} = \frac{2}{3}N^{2/3} \left(\log(2N) - 1.00401 + \frac{0.906526}{\log(2N)} \right)^{-1} \quad (8)$$

with $\kappa_{f\perp}$ and $\kappa_{f\parallel}$ the dynamic shape factor for a motion perpendicular, and parallel respectively, to the major axis of a straight chain of N -spheres.

To the authors knowledge, no experimental data are available for hydrodynamic torque acting on chain-like microrobot, while in our works an accurate theoretical calculation is particularly important. Therefore, based on numerical approximation conducted in [23], [24], we have correlated their results, using a nonlinear least-squares method, with a functional similar to the dynamic shape factor (7)-(8). Hence, we propose here the following model of the rotational shape factor for a motion perpendicular and parallel to the major axis of a straight chain of N -spheres:

$$\kappa_{\text{rot}\perp} = 0.3564 \cdot N^2 \left(\log(2N) - 1.046 + \frac{0.5069}{\log(2N)} \right)^{-1} \quad (9)$$

$$\kappa_{\text{rot}\parallel} = 0.0302 \cdot N^{1/9} \left(\log(2N) + 29.69 + \frac{1.8175}{\log(2N)} \right)^{-1} \quad (10)$$

The Fig. 3 depicts a comparison of this model with the BEM [24] and MEM [23] approximations for a chain of N -spheres up to $N = 15$. Reasonable agreement is seen between our model values wrt. values predicted with either the BEM or MEM. Especially, considering the BEM results, the root mean square error (RMSE) is 0.084 in direction perpendicular to the major axis, and 0.014 for parallel motion.

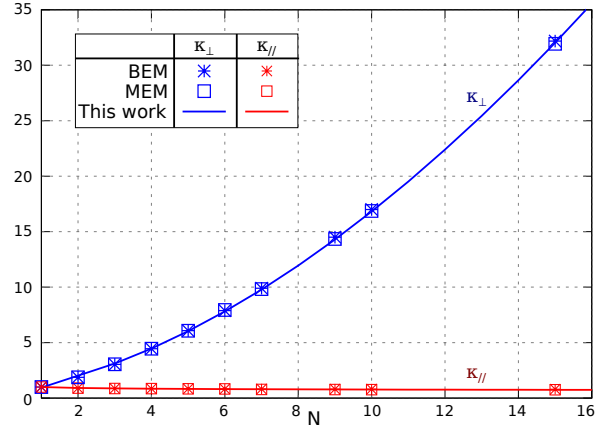


Fig. 3. Rotational shape factor $\boldsymbol{\kappa}_{\text{rot}}$ for chain-like microrobot, calculated by BEM [24], MEM [23], and our proposed model.

III. EXPERIMENTAL SETUP

To manipulate the chain-like magnetic microrobot an electromagnetic based actuation testbed (Aeon™, ETH Zürich) is used to generate the controlled rotating magnetic fields, and is depicted in Fig. 4. This setup comprises three nested sets of coils combined coaxially such that the magnetic field can be controlled in the center of the workspace [27]. The designed coils arrangement allows to generate homogeneous magnetic field $\mathbf{b} = (b_x, b_y, b_z)^T$ up to $\|\mathbf{b}\| = 35.7$ mT in a workspace of $20\text{mm} \times 20\text{mm}$ (see Fig. 6).

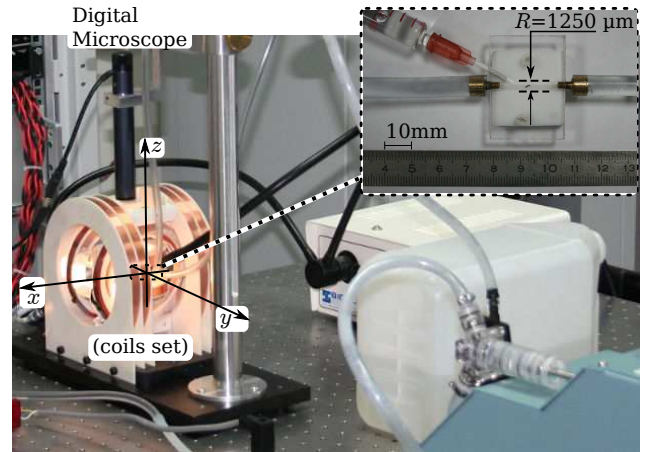


Fig. 4. Experimental setup with: the coils set; the digital microscope; and the microfluidic circuit.

Moreover, the magnetic setup is equipped with a CCD high-resolution digital microscope camera (TIMM 400, Nanosensor) providing up to $26\text{mm} \times 20\text{mm}$ field of view. A robust tracking algorithm measure, with a sub-micrometer resolution, the location of the center of gravity of the chain-like microrobot by real-time processing the video images acquired by the digital microscope.

Furthermore, the body of the chain-like microrobot is composed by spherical neodymium-iron-boron (neodymium magnet). A chain of this ferromagnetic microbeads were characterized under the field of view of an optical microscope

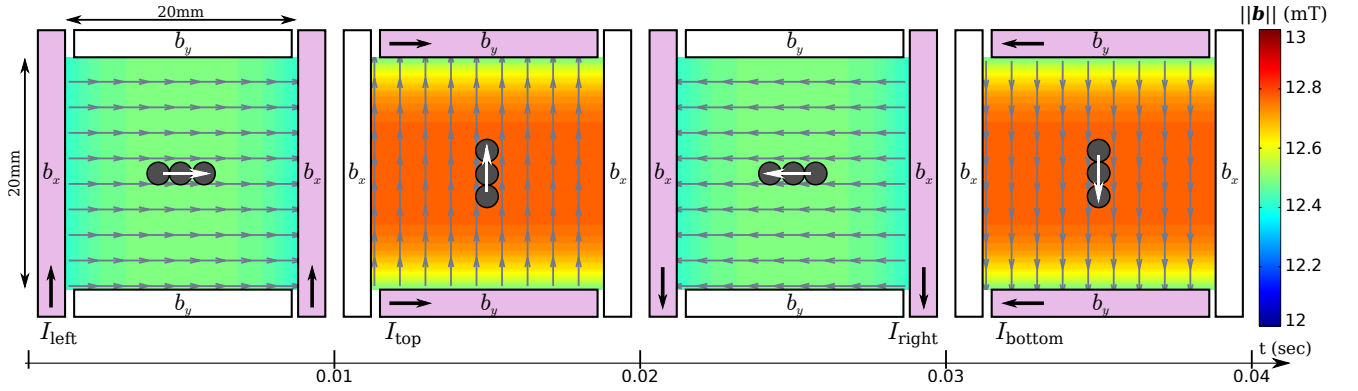


Fig. 6. Schematic overview of the timeline for the rotation of a chain of microspheres: at each step a pair of coils is crossed by a current $|I| = 12.5$ A flowing in the same direction generating an homogeneous magnetic field \mathbf{m} inside the workspace.

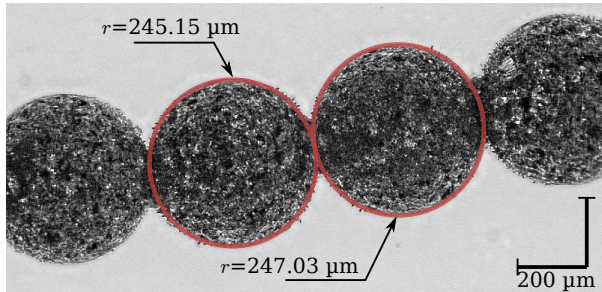


Fig. 5. Microscope view of the ferromagnetic chain-like microrobot.

as depicted in Fig. 5. The microscope imaging analysis helps to measure the radii of each microspheres, which are about $r = 245 \mu\text{m}$ ($\pm 1\%$). Table I summarizes the relevant experimental conditions used in the sequel.

TABLE I
EXPERIMENTAL CONDITIONS (at[†] $T = 20^\circ\text{C}$).

Microsphere	radius	r	$245 \mu\text{m}$
neodymium magnet (NdFeB - 35)	density	ρ_m	7500 kg/m^3
	magnetization	M	$1.23 \times 10^6 \text{ A/m}$
Aqueous mixture of 60% of glycerol	density	ρ	1173 kg/m^3
viscosity		η	$10.9 \text{ mPa}\cdot\text{s}$

[†]The experiments are conducted at air conditioned.

IV. MAGNETIC ROTATION OF CHAIN-LIKE MICROROBOT IN VISCOUS FLOW

A. Methods

First, the goal of this work is to investigate the rotational motion of a magnetic chain of microbeads. To this aim it is necessary to create an uniform rotating magnetic field. The experimental configuration of the coils set used to create a rotating magnetic field is shown in Fig. 4. A pair of coils allows to create an uniform magnetic field along its axis when an equal current I flows in the same direction, as illustrated in Fig. 6. For instance, when $I = 12.5$ A, in the x -axis pair of coils the magnitude of the magnetic field is $\|\mathbf{b}\| = 12.49 \text{ mT}$ with a standard deviation (StD) of $\sigma_{b_x} = 62.43 \mu\text{T}$ inside the workspace. Similarly, the y -axis pair of

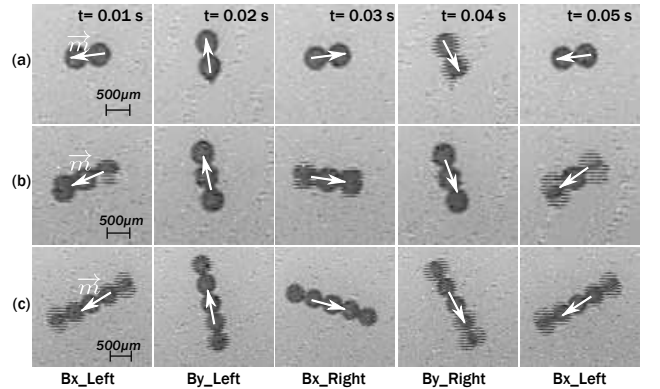


Fig. 7. Rotation motion control of a chain-like microrobot for $N = 2, 3$ and 5 microbeads.

coils generates a magnetic field of $\|\mathbf{b}\| = 12.78 \text{ mT}$ with a StD of $\sigma_{b_y} = 63.9 \mu\text{T}$. Let us notice that the difference between the x and y -axis is due to the different settings between the two pair of coils (e.g. coils radius and turns). Then, by changing the current direction, the magnetic field operates identically in the opposite direction. Thus, to create the rotating magnetic field each pair of coils are cyclically activated one after another. As example, Fig. 6 illustrates the rotation of the magnetic field in the clockwise direction leading to an angular velocity of $\omega_m = 314.16 \text{ rad/s}$.

B. Experimental Results

Fig. 7 shows a series of snapshots of typical rotation over time for three different ferromagnetic chain-like microrobot. The experiments were carried with several ferromagnetic beads with $245 \mu\text{m}$ of radii placed in a transparent box filled with an aqueous mixture of 60% of glycerol (cf. Table I). Under the influence of the magnetic field the magnetic microrobot tends to align its magnetization \mathbf{m} along the magnetic field \mathbf{b} to form a chain-like structure. When activating the coils set cyclically, the magnetic field and the chain rotates as well at the angular velocity ω_m . More precisely, at $t = 0$ when the magnetic field begins to rotate, the driving magnetic torque \mathbf{t}_m increases and thus speeds up the aggregate. This tends to increase the lag θ resulting in larger magnetic torque

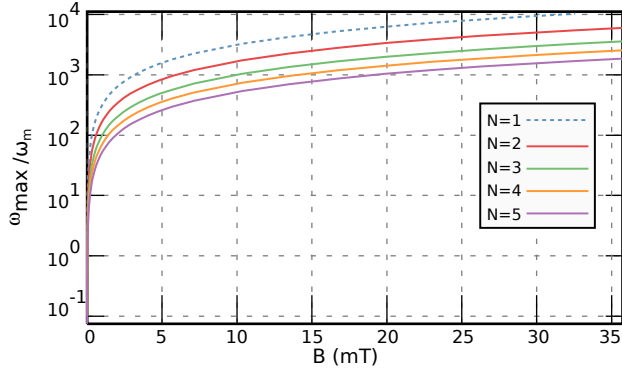


Fig. 8. Ratio between the maximum angular velocity ω_{\max} and the magnetic field angular velocity ω_m wrt. the magnetic field strength for chain-like microrobot composed with different number (N) of microbeads.

(2). But, the drag torque \mathbf{t}_d limits this grow, then the magnetic microrobot converges to a constant θ , and we get $\mathbf{t}_m = \mathbf{t}_d$. From (2) and (6) is straightforward to deduce that when $\theta = \pi/2$ the maximum angular velocity is obtained where $\mathbf{t}_m = \mathbf{t}_d$, and leads to:

$$\omega_{\max} = \frac{\|\mathbf{m}\| \|\mathbf{b}\|}{6\eta \kappa_{\text{rot}}} \quad (11)$$

Fig.8 presents the ratio ω_{\max}/ω_m wrt. the magnetic field strength. As long as the magnetic field angular velocity ω_m does not exceed ω_{\max} , synchronous rotation of chain-like microrobot is achieved. In opposition, if the magnetic field frequency is too high, the drag force acting on the microrobot surpasses the magnetic torque, and the synchronization is lost. In our context, the synchronization condition is fulfilled for magnetic field magnitude above about $\|\mathbf{b}\| > 1\mu\text{T}$. Especially, this assumption is validated experimentally in Fig. 7, where one can see that the rotational motion of the microrobots does not rely on the number of beads. Therefore, we can deduce that the maximum torque applied to the microrobot is independent of the magnetic field frequency, but is mainly related to the magnitude of the applied magnetic field in the workspace and to the size of the bead chain

V. AN UNCLOGGING STRATEGY FOR THE CHAIN-LIKE MAGNETIC MICROROBOT

A. Methods

The proposed magnetic microrobot could be useful in the treatment of arterial occlusive diseases (AOD), such as atherosclerosis or peripheral vascular disease. To this aims a microfluidic chips is designed to simulate a small artery with a radius of 1.25mm (see inlet in Fig. 4), and is filled with a mixture of 60% of glycerin and water leading to a fluid viscosity of $\eta = 10.9\text{mPa}\cdot\text{s}$ (cf. Table I). Then, an emulsion with varying concentrations of lipid and glass-fiber were injected into the phantoms to mimic regions of fibrous plaque containing calcification plaque. To propel efficiently the magnetic microrobot from an initial location to the clogged area, a first solution is to propel the microrobot using

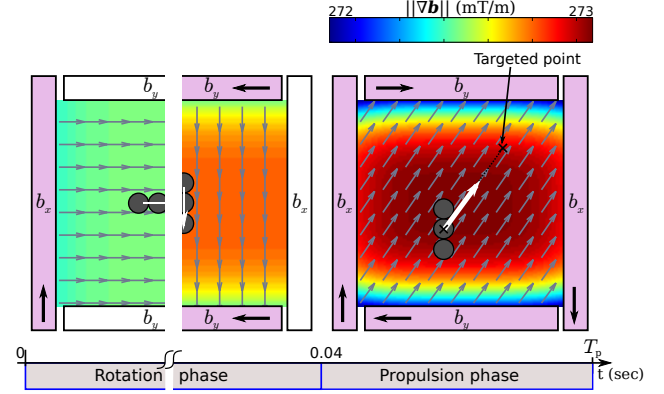


Fig. 9. Schematic overview of the timeline for the unclogging strategy: first a rotating phase (as in Fig. 6), and next a magnetic gradient steering phase.

magnetic gradient based on a simple proportional-integral-derivative (PID) controller [28], predictive controller [7] or adaptive backstepping controller [29]. Once the occluded region is reached, the proposed magnetic rotation could be applied. Another solution is to exploit the microrobot geometry and navigate close to the pipe wall to take advantage of the asymmetric boundary conditions. Indeed, in such condition the drag coefficient of the microrobot increases when it approaches a wall. Especially, if a rotational motion is applied a velocity difference between the two ends of the microrobot appears. Based on this consideration, Zhang *et al.* have propelled a Ni nanowire near a patterned solid surface [16]. However, it is not obvious to efficiently extend this methods to a chain-like structure with different number of microspheres. Furthermore, the proposed formalism is mainly devoted to non-contact manipulation. In this work, we propose a simpler alternative strategy, where the rotation motion sequence is extended to include a steering step as depicted in Fig.9. In these propulsion phase an uniform magnetic gradient $\nabla\mathbf{b}$ is generated inside the workspace as in [27] to drive the microrobot to the occluded targeted area. This strategy allows to alternate a rolling and pulling phases to mechanically unclog a fibrous plaque.

B. Experimental Results

Fig.10 illustrates a chronological series of snapshots of the unclogging strategy. The experiments are realized using a microrobot that is composed by a chain of three magnetic microspheres in a cylindrical pipe with a radius of 1.25mm. This result demonstrates the efficiency of the proposed technique to remove a plaque area that fully occluded the microfluidic circuit, as at t_5 this plaque is removed. Let us notice that only the fibrous tissue is visible (here in dark inside the circle), whereas the lipid component is not seen. Fig. 11a shows the path followed by the microrobot and by the fibrous plaque. Between instants t_0 to t_1 , the microrobot has first to reach the targeted occluded area using the proposed motion sequence. At time t_1 the microrobot collides with the plaque, with a magnetic force of $\|\mathbf{f}_m\| = 104.34\mu\text{N}$ due to the gradient steering (1), and a maximal magnetic

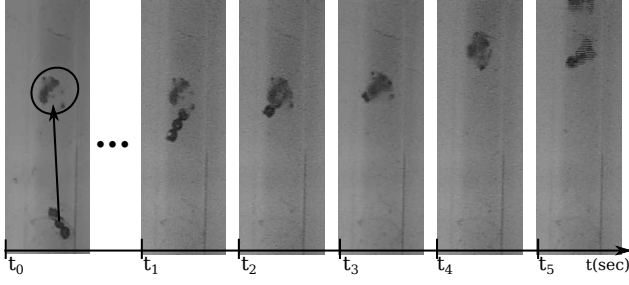


Fig. 10. Plaque removal chronology using a chain of three magnetic microspheres.

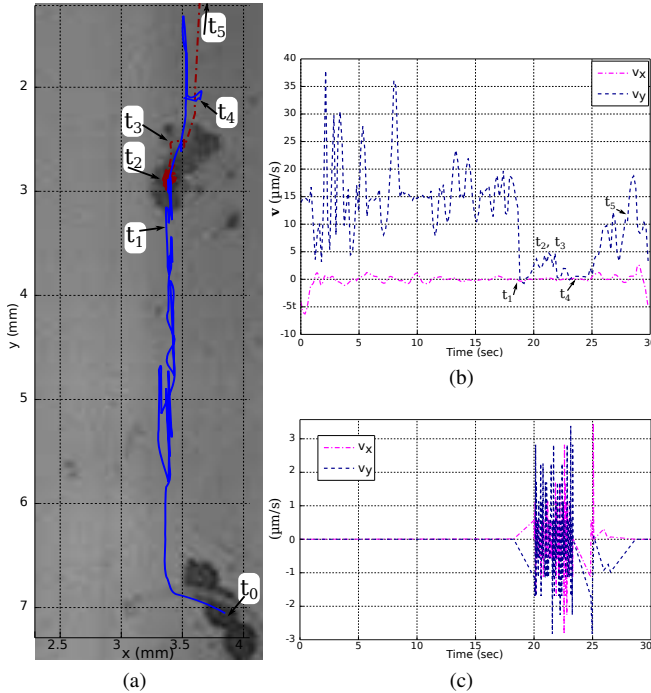


Fig. 11. Unclogging experiments: (a) the path followed by the magnetic microrobot (blue line) and by the plaque area (dashed line); the velocities of the (b) microrobot and (c) plaque tissue.

torque of $\|\mathbf{t}_m\| = 4.98 \mu\text{N} \cdot \text{m}$ due to the rotational motion (2). Here, the unclogging strategy consists in a rotating motion with a frequency of 25Hz followed by a gradient steering steps of 10ms. These two steps motions interlock the microrobot with the clogging material, and then it remains only an oscillating and pulling motions. During time t_1 to t_2 , this microrobot motion (cf. Fig. 11b) are not sufficient to move the plaque significantly, as depicted in Fig. 11c. From the instant t_3 , the incessant scraping motion of the microrobot is finally able to displace the fibrous plaque which start to slip from the pipe wall. As one can see the clogging material oscillate. This behavior is due to the oscillating motion of the microrobot. At time t_4 , the plaque clings to the wall once again and occlude the microfluidic circuit. The velocity of the plaque (cf. Fig. 11c, together with the microrobot velocity (cf. Fig. 11b), vanish. After all, at t_5 , the unclogging motion sequence of the microrobot successfully removed the occluding material from the microfluidic circuit.

Like most biological materials, atherosclerotic plaques are

mechanically and morphologically complex. In this paper, an emulsion with varying concentrations of lipid and glass-fiber is used as clogging material. The three-dimensional structure of the plaque suggests that mechanical properties such as stiffness vary with the direction of the imposed stress or strain. Nevertheless, the lipid component are not visible from the digital microscope imaging system. Therefore, it is difficult to measure efficiently the strain of the fibrous plaque. To analyze the stress-strain relation in the fibrous plaque more completely, further studies of plaque anisotropy will envisaged.

VI. CONCLUSION

This paper investigates the use of chain-like microrobot to expand the range of biomedical application. Different experiments have been realized. First the rotational behavior of the microrobot with different number of microspheres is characterized. This analysis helps to asses the validity of the model of the considered microrobot in viscous environment. Hence, the microrobot efficiency is experimentally demonstrated in the atherectomy case study. To this aims a simple unclogging motion sequence is proposed for fibrous plaque removing. Future extends will consider the stress-strain relation characterization.

REFERENCES

- [1] J. Abbott, Z. Nagy, F. Beyeler, and B. Nelson, "Robotics in the Small," *IEEE Robot. Automat. Mag.*, p. 92, 2007.
- [2] B. J. Nelson, I. K. Kaliakatsos, and J. J. Abbott, "Microrobots for minimally invasive medicine," *Annual Review of Bio.med. Eng.*, vol. 12, no. 1, pp. 55–85, 2010.
- [3] J. J. Abbott, K. E. Peyer, M. C. Lagomarsino, L. Zhang, L. X. Dong, I. K. Kaliakatsos, and B. J. Nelson, "How should microrobots swim?" *Int. J. of Robot. Res.*, Jul. 2009.
- [4] S. Martel, J.-B. Mathieu, O. Felfoul, A. Chanu, E. Aboussouan, S. Tamaz, P. Pouponneau, L. Yahia, G. Beaudoin, G. Soulez, and M. Mankiewicz, "Automatic navigation of an untethered device in the artery of a living animal using a conventional clinical magnetic resonance imaging system," *Applied Physics Letters*, vol. 90, no. 11, p. 114105, 2007.
- [5] S. Martel, M. Mohammadi, O. Felfoul, Z. Lu, and P. Pouponneau, "Flagellated magnetotactic bacteria as controlled MRI-trackable propulsion and steering systems for medical nanorobots operating in the human microvasculature," *Int. J. of Robot. Res.*, vol. 28, no. 4, pp. 571–582, 2009.
- [6] C. Dahmen, D. Folio, T. Wortmann, A. Kluge, A. Ferreira, and S. Fatikow, "Evaluation of a mri based propulsion/control system aiming at targeted micro/nano-capsule therapeutics," in *IEEE/RSJ Int. Conf. on Intel. Robots and Systems (IROS'2012)*, Vilamoura, Algarve, Portugal, Oct. 2012, pp. 2565–2570.
- [7] K. Belharet, D. Folio, and A. Ferreira, "Three-dimensional controlled motion of a microrobot using magnetic gradients," *Advanced Robotics*, vol. 25, no. 8, pp. 1069–1083(15), 2011.
- [8] L. Edd, S. Payen, B. Rubinsky, M. L. Stoller, and M. Sitti, "Biomimetic propulsion for a swimming surgical microrobot," *IEEE/RSJ Int. Conf. on Intel. Robots and Systems*, pp. 2583–2588, 2003.
- [9] L. Zhang, J. J. Abbott, L. Dong, B. E. Kratochvil, D. Bell, and B. J. Nelson, "Artificial bacterial flagella: Fabrication and magnetic control," *Applied Physics Letters*, vol. 94, no. 6, p. 064107, 2009.
- [10] R. Dreyfus, J. Baudry, M. L. Roper, M. Fermigier, H. A. Stone, and J. Bibette, "Microscopic artificial swimmers," *Nature*, vol. 437, no. 7060, pp. 862–865, 2005.
- [11] A. A. Evans and E. Lauga, "Propulsion by passive filaments and active flagella near boundaries," *Physical Review E*, vol. 82, no. 4, p. 041915, 2010.

- [12] L. Arcèse, M. Fruchard, and A. Ferreira, "Endovascular Magnetically-Guided Robots: Navigation Modeling and Optimization," *IEEE Trans. Biomed. Eng.*, vol. 59, no. 4, pp. 977–987, 2012.
- [13] K. E. Peyer, L. Zhang, and B. J. Nelson, "Bio-inspired magnetic swimming microrobots for biomedical applications," *Nanoscale*, vol. 5, no. 4, pp. 1259–1272, 2013.
- [14] H. Choi, J. Choi, S. Jeong, C. Yu, J. O. Park, and S. Park, "Two-dimensional locomotion of a microrobot with a novel stationary electromagnetic actuation system," *Smart Material and Structures*, vol. 18, p. 115017, 2009.
- [15] M. S. S. Floyd, C. Pawashe, "Two-dimensional contact and noncontact micromanipulation in liquid using untethered mobile magnetic micro-robot," *IEEE Trans. Robot.*, vol. 25, no. 6, pp. 303–308, 2009.
- [16] L. Zhang, T. Petit, Y. Lu, B. E. Kratochvil, K. E. Peyer, R. Pei, J. Lou, and B. J. Nelson, "Controlled propulsion and cargo transport of rotating nickel nanowires near a patterned solid surface," *ACS nano*, vol. 4, no. 10, pp. 6228–6234, 2010.
- [17] Q. A. Pankhurst, J. Connolly, S. K. Jones, and J. Dobson, "Applications of magnetic nanoparticles in biomedicine," *J. of Physics D: Applied Physics*, vol. 36, no. 13, pp. R167–181, 2003.
- [18] J. W. Maccoll, "Aerodynamics of a spinning sphere," *J. of the Royal Aeronautical Society*, vol. 28, pp. 777–798, 1928.
- [19] S. Dennis, D. Ingham, and S. Singh, "The steady flow of a viscous fluid due to a rotating sphere," *The Quarterly J. of Mechanics and Applied Mathematics*, vol. 34, no. 3, pp. 361–381, 1981.
- [20] G. Kasper, T. Niida, and M. Yang, "Measurements of viscous drag on cylinders and chains of spheres with aspect ratios between 2 and 50," *J. of aerosol science*, vol. 16, no. 6, pp. 535–556, 1985.
- [21] A. Unnikrishnan and R. Chhabra, "An experimental study of motion of cylinders in newtonian fluids: wall effects and drag coefficient," *The Canadian J. of Chemical Engineering*, vol. 69, no. 3, pp. 729–735, 1991.
- [22] S. N. Rogak and R. C. Flagan, "Stokes drag on self-similar clusters of spheres," *J. of colloid and interface science*, vol. 134, no. 1, pp. 206–218, 1990.
- [23] A. Filippov, "Drag and torque on clusters of n arbitrary spheres at low reynolds number," *J. of colloid and interface science*, vol. 229, no. 1, pp. 184–195, 2000.
- [24] A. Geller, L. Mondy, D. Rader, and M. Ingber, "Boundary element method calculations of the mobility of nonspherical particles—1. linear chains," *J. of aerosol science*, vol. 24, no. 5, pp. 597–609, 1993.
- [25] A. Hölzer and M. Sommerfeld, "Lattice boltzmann simulations to determine drag, lift and torque acting on non-spherical particles," *Computers & Fluids*, vol. 38, no. 3, pp. 572–589, 2009.
- [26] M. Zastawny, G. Mallouppas, F. Zhao, and B. Van Wachem, "Derivation of drag and lift force and torque coefficients for non-spherical particles in flows," *Int. J. of Multiphase Flow*, vol. 39, pp. 227–239, 2012.
- [27] K. Belharet, D. Folio, and A. Ferreira, "Control of a magnetic microrobot navigating in microfluidic arterial bifurcations through pulsatile and viscous flow," in *IEEE/RSJ Int. Conf. on Intel. Robots and Systems (IROS'2012)*, Vilamoura, Algarve, Portugal, Oct. 2012, pp. 2559–2564.
- [28] S. Tamaz, A. Chanu, J.-B. Mathieu, R. Gourdeau, and S. Martel, "Real-time mri-based control of a ferromagnetic core for endovascular navigation," *IEEE Trans. Bio-Med. Eng.*, vol. 55, no. 7, pp. 1854–1863, July 2008.
- [29] L. Arcese, M. Fruchard, and A. Ferreira, "Adaptive controller and observer for a magnetic microrobot," *IEEE Trans. Robot.*, vol. PP, no. 99, pp. 1–8, 2013.